JOURNAL OF Materials CHEMISTRY

Structure and magnetic properties of $Li_3Fe_2(AsO_4)_{3-x}(PO_4)_x$ [$x=0$, 1, 1.5, 2]: two sublattice weak ferromagnets

Jose Luis Mesa,[a] Aintzane Goñi,[a] Ana Lucia Brandl,[b] Nelson Orlando Moreno,[b] Gastón Eduardo Barberis[a,b] and Teófilo Rojo*[a]

[a]*Dpto. Química Inorgánica, F. Ciencias, UPV/EHU. Apdo 644, 48080 Bilbao, Spain. E-mail: qiproapt@lg.ehu.es*
[b]*Instituto de Física Gleb Wataghin, UNICAMP, 13087-970 Campinas (SP), Brazil*

Received 14th March 2000, Accepted 11th August 2000
First published as an Advance Article on the web 31st October 2000

The $Li_3Fe_2(AsO_4)_{3-x}(PO_4)_x$ ($x=0$, 1, 1.5, 2) solid solution was prepared by the ceramic method. $Li_3Fe_2(AsO_4)_3$ crystallizes in the monoclinic $P112_1/n$ space group with the cell parameters, $a=8.608(1)$, $b=12.215(1)$, $c=8.929(1)$ Å and $\gamma=90.76(1)^\circ$. The structure consists of a three-dimensional framework of vertex-sharing FeO_6 octahedra and AsO_4 tetrahedra with the lithium ions distributed in three four-coordinated crystal sites. There are two independent iron positions in the structure of this compound, Fe(1) and Fe(2). The cell parameters of the isostructural $Li_3Fe_2(AsO_4)_{3-x}(PO_4)_x$ ($x=0$, 1, 1.5, 2) phases follow Vegard's law. The IR spectra show the evolution of the intensity for the bands corresponding to the AsO_4 and PO_4 tetrahedra in the solid solution. An isotropic signal with a g value of 2.0 is observed in the ESR spectra of all compounds, in good agreement with the presence of a high spin Fe(III) ion with slightly distorted octahedral symmetry. The magnetization measurements and the magnetic DC and AC susceptibility data show an antiferromagnetic behavior for these compounds, with the presence of a ferromagnetic component below the ordering temperature. T_N decreases from 35.5 to 31 K with decreasing the amount of arsenate. The magnetic results are explained by the existence of a phenomenon of ferrimagnetism in these compounds, due to the existence of two different magnetic sublattices, corresponding to the Fe(1) and Fe(2) sites. The presence of canting between the magnetic moments of these two sublattices has been also detected. This fact agrees with the relative orientation of the FeO_6 magnetic octahedra in the $Li_3Fe_2(AsO_4)_{3-x}(PO_4)_x$ ($x=0$, 1, 1.5, 2) compounds.

Introduction

The $A_3Fe_2(XO_4)_3$ (A = Li, Na; X = P, As) compounds are well known as fast ionic conductors.[1–5] The structures of these phases are related to two different structure types: Nasicon type[6] for the sodium phases and $Fe_2(SO_4)_3$ type[7] for the lithium compounds. These structures present similar $[Fe_2(XO_4)_3]$ frameworks, constituted by corner-shared FeO_6 octahedra and XO_4 tetrahedra. However, the different space orientation of the polyhedra leads to changes in the symmetry of the systems. This fact does not affect the ionic conductivity properties of the phases, which present excellent values in all cases, but allows the existence of different and interesting magnetic behaviors in this family of compounds. In this sense, $Na_3Fe_2(PO_4)_3$[8–9] shows a magnetic transition at 47 K to a weakly ferromagnetic phase.[10] The remanent weak magnetic component, which is estimated to be about 2% of the total magnetic moment of the Fe(III) ions, is consistent with a small canting ($\approx 0.2^\circ$) of the antiferromagnetically coupled moments of the iron ions.[11,12]

$Fe_2(SO_4)_3$, representative of the other above mentioned structure type, also presents a weak ferromagnetic moment below the ordering temperature at 28 K. However, powder neutron diffraction, Mössbauer and magnetic studies indicated that this compound is a two sublattice antiferromagnet. Each sublattice is made up of crystallographically different iron ions in the monoclinic space group $P2_1/n$. So, the ferromagnetic component is a result of the ferrimagnetic coupling between the two different iron sublattices.[13] Similar ferromagnetic behavior has been observed for another related compound, $Fe_2(MoO_4)_3$.[14–17] However, $Li_2Fe_2(MoO_4)_3$,[18,19] synthesized *via* the topotactic redox-insertion reaction of LiI with $Fe_2(MoO_4)_3$, does not exhibit two iron sublattices but also shows a weakly ferromagnetic state below T_N due to an intrinsic canting of the iron magnetic moments.[20]

$Li_3Fe_2(PO_4)_3$, isostructural to $Fe_2(SO_4)_3$ and $Fe_2(MoO_4)_3$, shows the presence of two sublattices of Fe(III) ions. The ferromagnetic ordering inside each sublattice at 29 K and the simultaneous ferrimagnetic interaction between two different sublattices lead to the appearance of a weak ferromagnetic moment below T_N. This ferromagnetic component tends towards zero at 0 K, because the magnetic moments of both ferromagnetic sublattices tend to saturate the total value of the Fe(III) ions.[21]

In this paper we describe the crystal structure of $Li_3Fe_2(AsO_4)_3$ together with the spectroscopic and magnetic study on the $Li_3Fe_2(AsO_4)_{3-x}(PO_4)_x$ ($x=0$, 1, 1.5, 2) solid solution. These compounds exhibit interesting magnetic properties because they display the simultaneous presence of canting and ferrimagnetism.

Experimental

Synthesis of $Li_3Fe_2(AsO_4)_{3-x}(PO_4)_x$ ($x=0$, 1, 1.5, 2)

The $Li_3Fe_2(AsO_4)_{3-x}(PO_4)_x$ ($x=0$, 1, 1.5, 2) phases were prepared by the ceramic method. Stoichiometric amounts of $Fe(NO_3)_3{\cdot}9H_2O$, $H_2NH_4AsO_4$, $H_2NH_4PO_4$ and $LiOH{\cdot}H_2O$ reagents were homogenized in an agate mortar. The resulting mixtures were heated at 1073 K, with an intermediate

Table 1 Percentages of the elements found (and calculated) for $Li_3Fe_2(AsO_4)_{3-x}(PO_4)_x$ ($x=0$, 1, 1.5, 2)

	$Li_3Fe_2(AsO_4)_3$	$Li_3Fe_2(AsO_4)_2(PO_4)$	$Li_3Fe_2(AsO_4)_{1.5}(PO_4)_{1.5}$	$Li_3Fe_2(AsO_4)(PO_4)_2$
% Li	3.6(3.79)	4.0(4.12)	4.2(4.31)	4.4(4.51)
% Fe	20.2(20.33)	22.1(22.10)	23.2(23.11)	24.2(24.21)
% As	40.5(40.92)	29.5(29.65)	23.2(23.25)	16.2(16.24)
% P		5.9(6.13)	9.6(9.61)	13.1(13.43)

regrinding. The experimental contents of Li, Fe, As and P in the products were determined by Inductively Coupled Plasma-Atomic Emission Spectroscopy (ICP-AES). The percentages of the elements found and calculated are displayed in Table 1.

Refinement of the crystal structure of $Li_3Fe_2(AsO_4)_3$

X-Ray powder diffraction pattern of $Li_3Fe_2(AsO_4)_3$ was recorded on a Siemens D501 automated diffractometer, using graphite-monochromated Cu-Kα radiation. The data collection was made in the 5–109.5° 2θ range, every 0.02°, with 20 seconds per step. The structure was refined using the FULLPROF[22] program, modelling the peak shape with a pseudo-Voigt function. The structural parameters of $Li_3Fe_2(PO_4)_3$[3] were used as a starting model for the Rietveld refinement. Scale and background variables were refined initially, followed in subsequent iterations by the zero point of 2θ, the cell constants and the peak-shape parameters. The atomic parameters were refined one by one in different stages starting with those corresponding to the elements of the highest scattering factors. From successive refinement cycles the reliability factors dropped to the values shown in Table 2. The experimental, calculated and difference XRD patterns of the $Li_3Fe_2(AsO_4)_3$ polycrystalline sample are shown in Fig. 1. Crystal parameters and details of the data collection and the structural refinement are given in Table 2. Tables 3 and 4 show the final atomic coordinates and selected bond distances and angles of $Li_3Fe_2(AsO_4)_3$, respectively.

Characterization and physical measurements

Analytical measurements were carried out by Inductively Coupled Plasma Atomic Emission Spectroscopy (ICP-AES) analysis, with an ARL 3410+ICP with Minitorch equipment. X-Ray powder diffraction patterns of $Li_3Fe_2(AsO_4)_{3-x}(PO_4)_x$ ($x=1$, 1.5, 2) were recorded on a Philips Xpert diffractometer, in the 5–70° 2θ range, every 0.02°, with 10 seconds per step. Infrared spectra were performed with a Nicolet FT-IR 740 spectrometer using the KBr disk technique. ESR spectra were carried out in a conventional ELXSYS Bruker X-band spectrometer using a TE102 room temperature cavity. The temperature of the samples was varied using a helium gas flux system with a temperature controller. Magnetization and magnetic susceptibility measurements were performed with a Quantum Design MPMS-2 SQUID Magnetometer, in the 1.8–300 K temperature range, with a maximum applied field of 7 T. AC susceptibility measurements were performed at 1 Oe and 1 kHz, on a Quantum Design PPMS AC susceptometer.

Table 2 Crystal parameters and details of the structure refinement of $Li_3Fe_2(AsO_4)_3$

Crystal system	Monoclinic
Space group	$P112_1/n$ (no. 14)
FW/g mol^{-1}	549.62
a/Å	8.608(1)
b/Å	12.215(1)
c/Å	8.929(1)
γ/°	90.76(1)
V/Å^3	938.8(1)
Z	4
T/K	295
Diffractometer	Siemens
Radiation (λ_1, λ_2/Å)	Cu-Kα (1.5406, 1.5444)
2θ/° range	5–109.5
Step/°	0.02
Time for step/s	20
No. of reflections	2320
No. of fitted parameters	71
R_F	7.52%
R_B	6.14%
R_p	7.66%
R_{wp}	10.2%

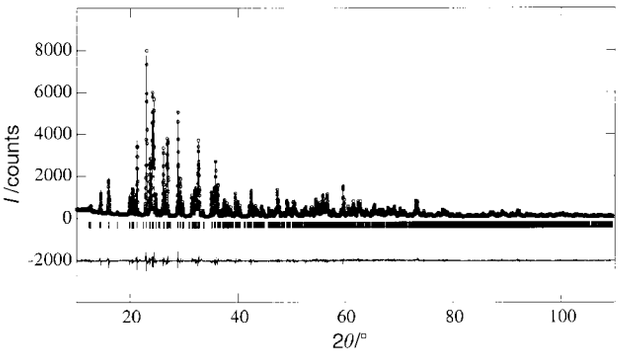

Fig. 1 Experimental, calculated and difference XRD patterns of the $Li_3Fe_2(AsO_4)_3$ polycrystalline sample.

Results

Crystal structure of $Li_3Fe_2(AsO_4)_3$

$Li_3Fe_2(AsO_4)_3$ is isostructural with the related phosphate $Li_3Fe_2(PO_4)_3$. The structure can be described as a three-dimensional framework of vertex-sharing FeO_6 octahedra and AsO_4 tetrahedra (Fig. 2). Each FeO_6 octahedron is surrounded by six AsO_4 tetrahedra and each tetrahedron is linked to four FeO_6 polyhedra making up the $[Fe_2(AsO_4)_3]^{3-}$ open framework. The lithium ions are distributed in three different crystal sites in the structure, filling the voids inside the iron arsenate structure and compensating the negative charge.

There are two independent iron positions in the structure of this compound, Fe(1) and Fe(2), which lead to the existence of two different FeO_6 octahedra (Fig. 3a). Both FeO_6 polyhedra present the six crystallographically independent oxygen atoms, because the identity is the unique symmetry element in the octahedra. So, for the Fe(1)O_6 octahedron, the six distances Fe(1)–O are quite different, ranging from 1.860(2) to

Table 3 Fractional atomic coordinates and B_{eq} temperature factors ($\times 10^2$ Å^2) for $Li_3Fe_2(AsO_4)_3$

Atom	x	y	z	B_{eq}
Fe(1)	0.2481(6)	0.1095(4)	0.4700(5)	0.3
Fe(2)	0.7449(6)	0.3947(4)	0.4765(5)	0.3
As(1)	0.1118(4)	0.1446(2)	0.1175(4)	0.3
As(2)	0.6149(4)	0.3503(3)	0.1226(4)	0.3
As(3)	0.0378(3)	0.4914(3)	0.2483(4)	0.3
O(1)	0.426(2)	0.304(1)	0.080(2)	0.7
O(2)	0.931(2)	0.093(1)	0.114(2)	0.7
O(3)	0.370(2)	0.255(1)	0.483(2)	0.7
O(4)	0.753(2)	0.226(1)	0.523(2)	0.7
O(5)	0.246(2)	0.057(1)	0.051(2)	0.7
O(6)	0.637(2)	0.484(1)	0.084(2)	0.7
O(7)	0.446(2)	0.064(1)	0.388(2)	0.7
O(8)	0.935(2)	0.388(1)	0.340(2)	0.7
O(9)	0.196(2)	0.432(1)	0.180(2)	0.7
O(10)	0.597(2)	0.091(1)	0.134(2)	0.7
O(11)	0.174(2)	0.193(1)	0.287(2)	0.7
O(12)	0.620(2)	0.333(1)	0.309(2)	0.7
Li(1)	0.321(6)	0.325(4)	0.270(6)	1.8
Li(2)	0.566(6)	0.205(4)	0.400(5)	1.8
Li(3)	0.061(6)	0.341(4)	0.504(5)	1.8

Table 4 Selected bond distances (Å) and angles (°) for $Li_3Fe_2(AsO_4)_3$

Iron coordination polyhedra					
Fe(1)		Fe(2)			
Fe(1)–O(3)	2.054(1)	Fe(2)–O(4)	2.105(1)		
Fe(1)–O(7)	1.943(3)	Fe(2)–O(8)	2.043(4)		
Fe(1)–O(11)	2.035(5)	Fe(2)–O(12)	1.983(5)		
Fe(1)–O(1)	2.090(3)	Fe(2)–O(2)	1.955(4)		
Fe(1)–O(9)	2.006(6)	Fe(2)–O(10)	1.964(4)		
Fe(1)–O(6)	1.860(2)	Fe(2)–O(5)	1.999(1)		
O(3)–Fe(1)–O(6)	168.2(3)	O(4)–Fe(2)–O(5)	175.2(2)		
O(7)–Fe(1)–O(1)	163.5(1)	O(8)–Fe(2)–O(2)	176.9(2)		
O(11)–Fe(1)–O(9)	163.0(1)	O(12)–Fe(2)–O(10)	160.8(1)		
O(3)–Fe(1)–O(7)	80.0(1)	O(4)–Fe(2)–O(8)	92.4(1)		
O(3)–Fe(1)–O(11)	76.8(1)	O(4)–Fe(2)–O(12)	78.6(1)		
O(7)–Fe(1)–O(11)	97.2(2)	O(8)–Fe(2)–O(12)	87.9(2)		
O(9)–Fe(1)–O(7)	93.8(2)	O(10)–Fe(2)–O(8)	83.1(1)		
O(1)–Fe(1)–O(11)	83.9(1)	O(2)–Fe(2)–O(10)	94.4(2)		
Arsenate tetrahedra					
As(1)		As(2)		As(3)	
As(1)–O(5)	1.691(2)	As(2)–O(1)	1.753(2)	As(3)–O(9)	1.669(3)
As(1)–O(11)	1.710(5)	As(2)–O(6)	1.676(1)	As(3)–O(8)	1.737(3)
As(1)–O(2)	1.673(2)	As(2)–O(12)	1.680(6)	As(3)–O(7)	1.707(4)
As(1)–O(3)	1.724(4)	As(2)–O(4)	1.723(3)	As(3)–O(10)	1.680(4)
O(5)–As(1)–O(11)	108.4(2)	O(1)–As(2)–O(6)	111.1(1)	O(9)–As(3)–O(8)	105.4(1)
O(5)–As(1)–O(2)	113.5(1)	O(1)–As(2)–O(12)	101.6(2)	O(9)–As(3)–O(7)	110.7(3)
O(5)–As(1)–O(3)	98.6(2)	O(1)–As(2)–O(4)	109.3(2)	O(9)–As(3)–O(10)	107.4(1)
O(2)–O(3)	2.770(3)	O(1)–O(4)	2.836(2)	O(9)–O(8)	2.710(4)
O(2)–O(5)	2.813(2)	O(1)–O(6)	2.828(1)	O(9)–O(7)	2.777(2)
O(2)–O(11)	2.862(4)	O(6)–O(12)	2.730(4)	O(9)–O(10)	2.700(4)
O(3)–O(5)	2.590(2)	O(12)–O(1)	2.660(5)	O(8)–O(7)	2.963(4)
O(5)–O(11)	2.758(4)	O(6)–O(4)	2.796(1)	O(7)–O(10)	2.630(5)
O(11)–O(3)	2.814(6)	O(12)–O(4)	2.869(5)	O(8)–O(10)	2.839(1)
Lithium coordination polyhedra					
Li(1)		Li(2)		Li(3)	
Li(1)–O(1)	1.935(5)	Li(2)–O(3)	1.947(3)	Li(3)–O(8)	1.919(5)
Li(1)–O(3)	2.129(4)	Li(2)–O(4)	1.969(4)	Li(3)–O(1)	1.909(2)
Li(1)–O(9)	1.882(3)	Li(2)–O(7)	1.991(1)	Li(3)–O(5)	2.104(2)
Li(1)–O(11)	2.040(1)	Li(2)–O(12)	1.820(3)	Li(3)–O(10)	1.981(4)

2.090(3) Å. The angles O–Fe(1)–O are rather deviated from the ideal ones (Table 4). The Fe(1) ion is located out of the equatorial plane formed by O(1), O(11), O(7) and O(9) oxygen atoms, as can be deduced by the deviation from 360° found in the sum of the four equatorial angles O–Fe(1)–O, which is equal to 356.8°. The Fe(2)–O bond distances and O–Fe(2)–O angles calculated for the $Fe(2)O_6$ octahedron are comparatively more regular than those corresponding to $Fe(1)O_6$. The six independent distances Fe(2)–O range from 1.955(4) to 2.105(1) Å, and the O–Fe(2)–O angles present values slightly closer to 90° (or 180°, for the axial angles). The Fe(2) ion can be considered as located inside the plane formed by the O(2), O(8) and O(10) atoms. The fourth equatorial oxygen, O(12), is out of the plane as a consequence of the polyhedral distortion.

Fig. 3a shows the tilt angles between both independent iron octahedra in the structure. In Fig. 3b the disposition of the two FeO_6 polyhedra in the related $Li_3Fe_2(PO_4)_3$ compound are shown for comparison. As can be observed, in the phosphate compound both independent octahedra are pseudosymmetrically related by a glide plane on *ac*. However, this pseudosymmetry is absent in the case of the arsenate compound, mainly due to the different space orientation of the polyhedra.

With respect to the arsenate groups, three distorted independent arsenate tetrahedra can be observed in the structure of $Li_3Fe_2(AsO_4)_3$. The As–O distances and the O–As–O angles present a wide range of values (see Table 4). These distortions can be attributed to the fact that all oxygen vertices in the $(AsO_4)^{3-}$ tetrahedra belong to different FeO_6 octahedra.

The lithium ions in the structure of this compound are four-coordinated to oxygen atoms with four different Li–O distances for each case (Table 4). The O–Li–O angles are quite deviated from 109° and, consequently the LiO_4 polyhedra cannot be considered as regular tetrahedra. It is interesting to note that the lithium sites in the structure of the related phosphate $Li_3Fe_2(PO_4)_3$, at room temperature, are rather different. In the latter compound, two of the lithium ions are five-coordinated and located inside trigonal bipyramids.

Crystallographic study of the $Li_3Fe_2(AsO_4)_{3-x}(PO_4)_x$ ($x=0$, 1, 1.5, 2) solid solution

The $Li_3Fe_2(AsO_4)_{3-x}(PO_4)_x$ ($x=1$, 1.5, 2) phases are isostructural with the parents $Li_3Fe_2(AsO_4)_3$ and $Li_3Fe_2(PO_4)_3$. All of them crystallize in the monoclinic $P112_1/n$ space group. The cell

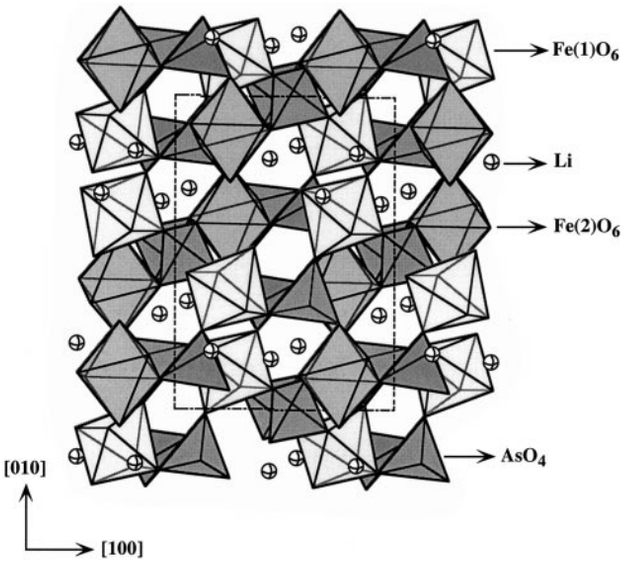

Fig. 2 Crystal structure of $Li_3Fe_2(AsO_4)_3$.

parameters (Table 5) exhibit a linear variation with the arsenate substitution degree, x, following Vegard's law. These parameters and the cell volume decrease in the solid solution with the gradual arsenate substitution by phosphate (see Fig. 4). This result is in good agreement with the periodic trend in radii down Group 15.

Infrared spectroscopy

The IR spectra of the title compounds show two important sets of bands (Fig. 5), which correspond to the arsenate and phosphate groups. The bands observed in the 980–760 cm^{-1} region are attributed to the stretching vibration modes of the AsO_4 groups. These bands are strong, broad and split in the case of the $Li_3Fe_2(AsO_4)_3$ phase due to the presence of three different AsO_4 tetrahedra in the structure. In the other phases, the gradual substitution of the arsenate by phosphate induces the appearance of another set of bands, in the 1200–950 cm^{-1} region, corresponding to the stretching vibration modes of the PO_4 groups. As expected, the relative intensity of these two sets of bands increases with the degree of arsenate–phosphate substitution.

A similar behavior is observed for the bending vibration modes of the AsO_4 and PO_4 tetrahedra. The bands appearing in the range from 550 to 430 cm^{-1} assigned to the symmetrical and asymmetrical deformation modes of the arsenate tetrahedra can be clearly observed for the $Li_3Fe_2(AsO_4)_3$ phase. However, the intensity of these bands decreases with the amount of arsenate substituted by phosphate. Simultaneously, another set of bands appears at 650–550 cm^{-1}, which can be attributed to the deformation modes of the PO_4 groups. The wavenumber values observed for all these signals are in good agreement with those given in the literature for these kinds of compounds.[23]

Table 5 Cell parameters for the $Li_3Fe_2(AsO_4)_{3-x}(PO_4)_x$ ($x=0$, 1, 1.5, 2, 3) compounds

x	a/Å	b/Å	c/Å	γ/°	V/Å^3
0	8.608(1)	12.215(1)	8.929(1)	90.76(1)	938.8(1)
1	8.635(2)	12.181(1)	8.807(3)	90.74(1)	926.3(1)
1.5	8.599(2)	12.121(1)	8.764(1)	90.65(2)	913.4(1)
2	8.595(1)	12.090(2)	8.708(1)	90.60(1)	904.8(1)
3[a]	8.562(2)	12.005(2)	8.612(2)	90.51(3)	885.2(1)

[a]From ref. 3.

ESR and magnetic properties

The powder X-band ESR spectra of the $Li_3Fe_2(AsO_4)_{3-x}(PO_4)_x$ ($x=0$, 1, 1.5, 2) compounds were measured at different temperatures from 296 to 5 K. Three selected spectra corresponding to $Li_3Fe_2(AsO_4)_{1.5}(PO_4)_{1.5}$ have been represented in the inset of Fig. 6, as an example. An isotropic signal with a g value of 2.0 is observed at room temperature in all cases, which is consistent with the presence of a high spin Fe(III) ion in a slightly distorted octahedral symmetry. No significant variation of the g value is observed over the whole temperature range for any phase. The integrated intensity of the absorption curve increases with decreasing temperature reaching a maximum in the temperature range from 36 to 31 K and after that rapidly decreases, becoming silent below 30 K.

The temperature dependence of the linewidth of the signals calculated by simulations of the experimental spectra to Lorentzian curves is displayed in Fig. 6. The linewidth is observed to have low temperature dependence between RT and 50 K for all compounds, probably due to the dipolar homogeneous broadening. Below this temperature the linewidth increases rapidly when the temperature is decreased reaching different maxima depending on the x content. This behavior indicates the establishment of the magnetic ordering in the compounds,[24] allowing us to deduce the temperatures of the critical point for each phase: 36 K for $Li_3Fe_2(AsO_4)_3$; 33 K for $Li_3Fe_2(AsO_4)_2(PO_4)$; 32 K for $Li_3Fe_2(AsO_4)_{1.5}(PO_4)_{1.5}$ and 31 K for $Li_3Fe_2(AsO_4)(PO_4)_2$. Consequently, the ordering temperature in the $Li_3Fe_2(AsO_4)_{3-x}(PO_4)_x$ ($x=0$, 1, 1.5, 2) solid solution decreases with increasing phosphate content, x, indicating the presence of higher magnetic interactions in the arsenate phase.

The molar magnetic susceptibility measurements of Li_3Fe_2

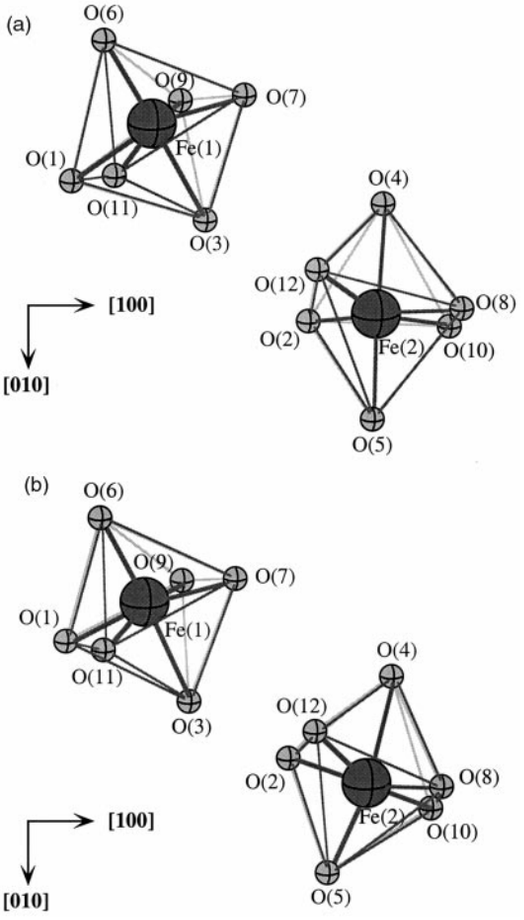

Fig. 3 View of the two crystallographically different FeO_6 octahedra in the structure of (a) $Li_3Fe_2(AsO_4)_3$ and (b) $Li_3Fe_2(PO_4)_3$.

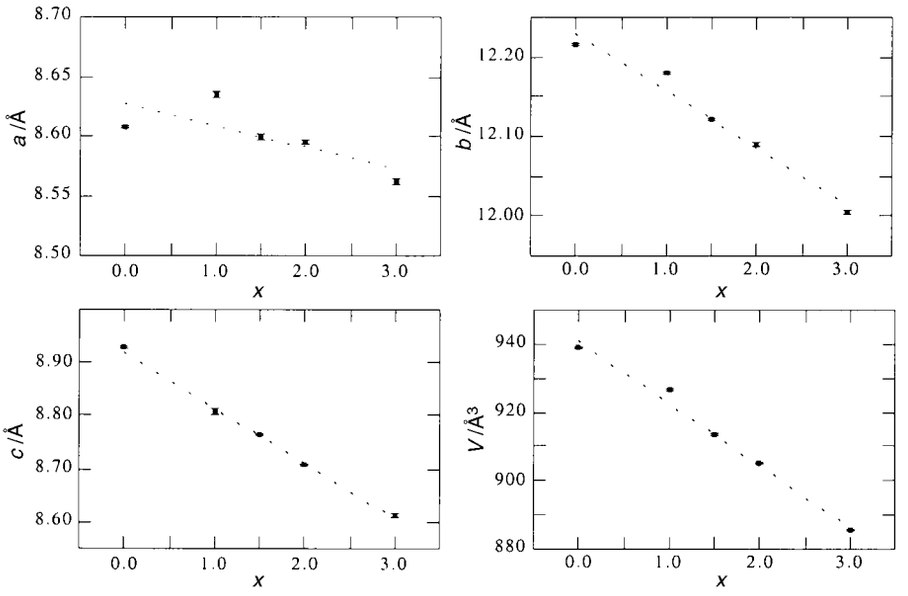

Fig. 4 Evolution of the cell parameters with the phosphate content, x, in the $Li_3Fe_2(AsO_4)_{3-x}(PO_4)_x$ solid solution.

$(AsO_4)_{3-x}(PO_4)_x$ ($x=0$, 1, 1.5, 2) were carried out in the temperature range 1.8–300 K, at a 0.1 T magnetic field. The high temperature data are not well described by a Curie–Weiss law in all cases. The $\chi_m T$ *vs.* T curves in the temperature range from 100 to 1.8 K are shown in Fig. 7. The $\chi_m T$ product diminishes with decreasing temperature from 300 K, indicating the predominance of antiferromagnetic interactions in all compounds. The $\chi_m T$ curves for all phases exhibit a minimum followed by a maximum whose values are given in Table 6. This behavior is characteristic of antiferromagnetic arrangements with the presence of a ferromagnetic component below the ordering temperature. The AC susceptibility data, represented in Fig. 8, accurately show the T_N value for each compound (Table 6). The ferromagnetic component which appears in the magnetic arrangement for all phases is revealed by the peak in the imaginary susceptibility χ''_m that accompanies the peak in χ'_m at T_N.

Magnetization *vs.* applied magnetic field measurements for $Li_3Fe_2(AsO_4)_{3-x}(PO_4)_x$ at 25 K (Fig. 9) show hysteresis loops, confirming the existence of a weak ferromagnetic behavior at this temperature. However, some differences can be seen for the different compounds. The $Li_3Fe_2(AsO_4)_3$ phase exhibits a lower value of coercive field than those of the other phases. The evolution of the magnetization values indicates that the resistance of the magnetic moments to the applied magnetic field increases with decreasing phosphate content, x.

In order to determine the thermal evolution of the remanent magnetization below the critical temperature, field-cooled (FC) magnetization *vs.* temperature measurements were also carried out. The samples were cooled with a field of 0.1 T and heated from 5 up to 50 K at zero field. The plot of the obtained curves is given in Fig. 10. As can be observed, there is a rapid increase of M just below T_N, reaching a different maximum value for each phase in the 30–20 K temperature range (Table 6). After that, the remanent magnetization (M_r) decreases with decreasing temperature in all cases, tending to different magnetization values when the temperature tends towards zero. The value observed is higher for the arsenate phase.

Discussion and conclusions

The $Li_3Fe_2(AsO_4)_{3-x}(PO_4)_x$ phases contain eight FeO_6 octahedra in the unit cell. Four of them correspond to the Fe(1) independent crystallographic site and the rest to the other site, Fe(2). These octahedra exhibit different polyhedral distortions with significant differences in the distances and angles. The

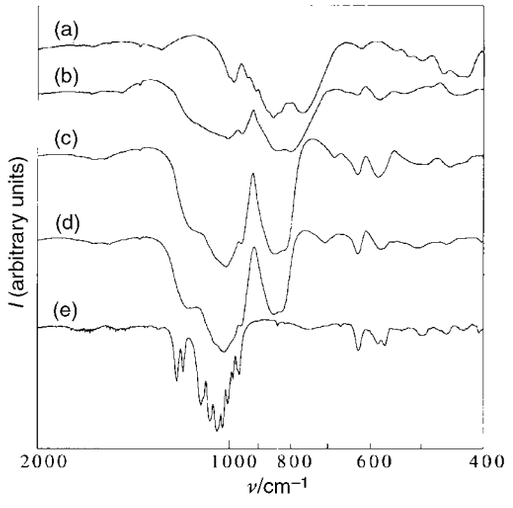

Fig. 5 IR spectra of (a) $Li_3Fe_2(AsO_4)_3$, (b) $Li_3Fe_2(AsO_4)_2(PO_4)$, (c) $Li_3Fe_2(AsO_4)_{1.5}(PO_4)_{1.5}$ (d) $Li_3Fe_2(AsO_4)(PO_4)_2$ and (e) $Li_3Fe_2(PO_4)_3$ (included for comparison).

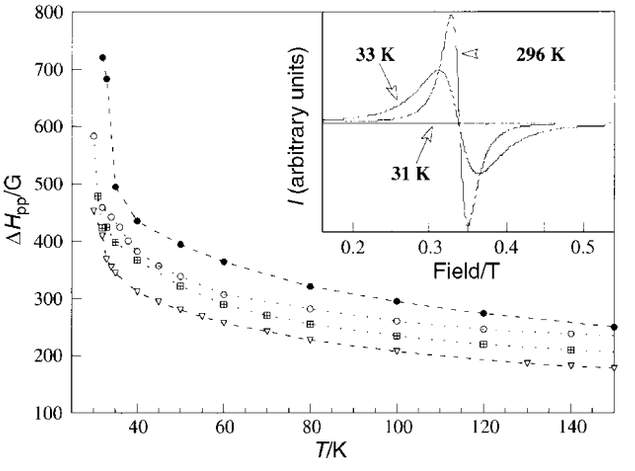

Fig. 6 Thermal evolution of the ESR linewidth, ΔH_{pp}, for -●- $Li_3Fe_2(AsO_4)_3$, -○- $Li_3Fe_2(AsO_4)_2(PO_4)$, -⊞- $Li_3Fe_2(AsO_4)_{1.5}(PO_4)_{1.5}$ and -▽- $Li_3Fe_2(AsO_4)(PO_4)_2$. Inset: three selected ESR spectra of $Li_3Fe_2(AsO_4)_{1.5}(PO_4)_{1.5}$ at different temperatures.

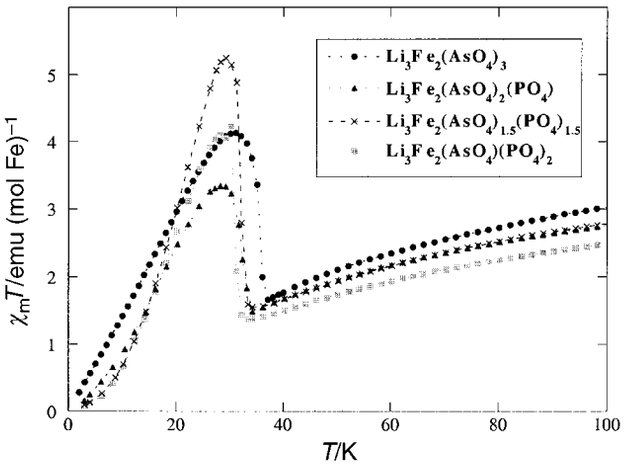

Fig. 7 Thermal evolution of the $\chi_m T$ product for $Li_3Fe_2(AsO_4)_{3-x}(PO_4)_x$ ($x=0$, 1, 1.5, 2), at 0.1 T.

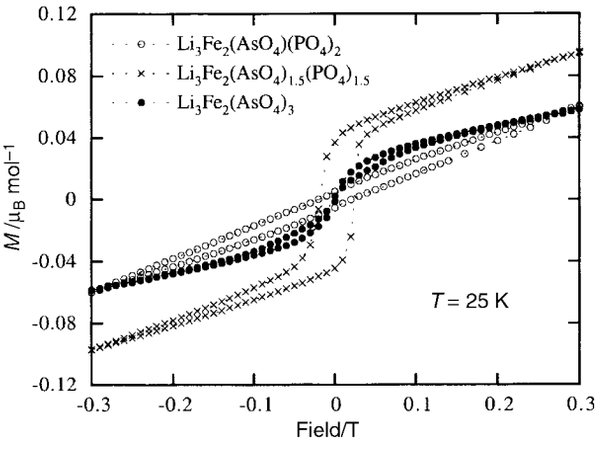

Fig. 9 Magnetization *versus* applied magnetic field at 25 K for $Li_3Fe_2(AsO_4)_{3-x}(PO_4)_x$ ($x=0$, 1.5, 2).

space orientation of two independent $Fe(1)O_6$ and $Fe(2)O_6$ octahedra shows changes in the $Li_3Fe_2(AsO_4)_{3-x}(PO_4)_x$ solid solution. Both independent octahedra are pseudosymmetric by a glide plane in $Li_3Fe_2(PO_4)_3$ whereas they are completely asymmetric in $Li_3Fe_2(AsO_4)_3$. In this sense, one could deduce that the tilt angle between $Fe(1)O_6$ and $Fe(2)O_6$ increases progressively with the arsenate content in this family of compounds.

The FeO_6 octahedra in the $Li_3Fe_2(AsO_4)_{3-x}(PO_4)_x$ ($x=0$, 1, 1.5, 2, 3) phases are linked together through AsO_4 or PO_4 groups, building the three-dimensional framework. So, the magnetic exchange pathways are established through the AsO_4 and PO_4 tetrahedra. The Fe–Fe interactions are intrinsically antiferromagnetic for all compounds. There is a significant decrease of T_N with increasing degree of arsenate–phosphate substitution, x. Considering the presence of similar magnetic exchange pathways for all phases, these results cannot be explained in a satisfactory way by the differences observed in distances and angles for both $Li_3Fe_2(AsO_4)_3$ and $Li_3Fe_2(PO_4)_3$ compounds. Consequently, the most significant factor must be attributed to the different relative orientation of the FeO_6 octahedra in the structure. This orientation affects the effectiveness of the overlap integral between the magnetic orbitals leading to the presence of strongest Fe–Fe interactions for $Li_3Fe_2(AsO_4)_3$.

Taking into account that the Fe(III) cations are arranged in two inequivalent sites, Fe(1) and Fe(2), the existence of two different magnetic sublattices can be considered. The antiferromagnetic coupling between Fe(1) and Fe(2) requires that each separate sublattice must be ferromagnetically coupled. Furthermore, the magnetic coupling constants from the two sublattices should be different (J_1 and J_2 for the Fe(1) and Fe(2) sublattices, respectively) as a consequence of the different values observed in distances and angles for the Fe(1)–Fe(1) and Fe(2)–Fe(2) superexchange pathways. Consequently, the weak ferromagnetic component observed below the ordering temperature for all phases can be explained by an incomplete compensation of the antiparallel magnetic moments of both Fe(1) and Fe(2) sublattices. It should be mentioned that the existence of weak ferrimagnetism in $Li_3Fe_2(AsO_4)_{3-x}(PO_4)_x$ ($x=0$, 1, 1.5, 2) agrees with the analysis of the magnetic behavior in the $Li_3Fe_2(PO_4)_3$ related compound.[21]

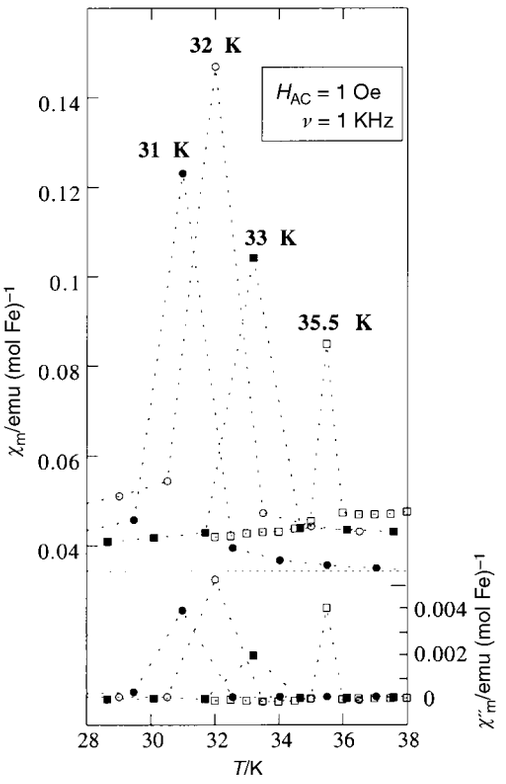

Fig. 8 Thermal evolution of the AC susceptibility for -□- $Li_3Fe_2(AsO_4)_3$, -■- $Li_3Fe_2(AsO_4)_2(PO_4)$, -○- $Li_3Fe_2(AsO_4)_{1.5}(PO_4)_{1.5}$ and -●- $Li_3Fe_2(AsO_4)(PO_4)_2$ from 28 to 38 K.

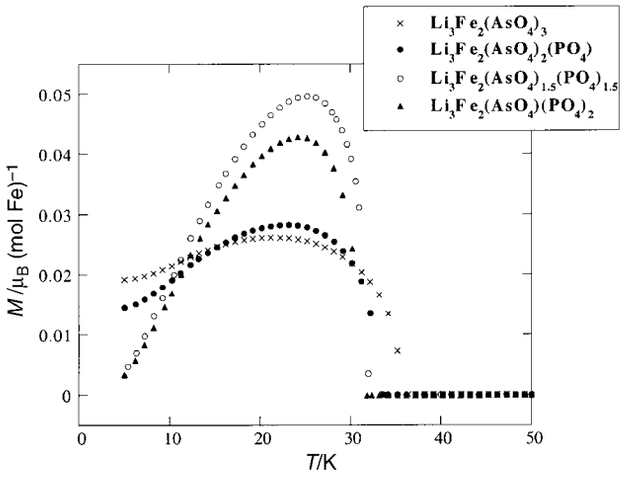

Fig. 10 Thermal evolution of the magnetization from 5 to 50 K. The $Li_3Fe_2(AsO_4)_{3-x}(PO_4)_x$ ($x=0$, 1, 1.5, 2) samples were previously field cooled at 0.1 T.

Table 6 Selected magnetic data for the $Li_3Fe_2(AsO_4)_{3-x}(PO_4)_x$ ($x=0$, 1, 1.5, 2) compounds

	$Li_3Fe_2(AsO_4)_3$	$Li_3Fe_2(AsO_4)_2(PO_4)$	$Li_3Fe_2(AsO_4)_{1.5}(PO_4)_{1.5}$	$Li_3Fe_2(AsO_4)(PO_4)_2$
[a]$T(\chi_m T)_{min}$/K	37	34	33.5	33
$T(\chi_m T)_{max}$/K	31	29	29	30
T_N/K	35.5	33	32	31
[b]H_c ($\times 10^{-4}$T)	20	170	210	200
M_r/μ_B (mol Fe)$^{-1}$	0.002	0.025	0.045	0.005
[c]T of M_{max}/K	22	23	25	24
M_{max}/μ_B (mol Fe)$^{-1}$	0.026	0.028	0.050	0.043
M at $T\rightarrow 0$ K/μ_B (mol Fe)$^{-1}$	0.019	0.015	0.004	0.003

[a]Data obtained from the $\chi_m T$ *versus* T curves, at 0.1 T. [b]Data obtained from the M *versus* H curves, at 25 K. [c]Data obtained from the M *versus* T curves of the 0.1 T FC samples.

The highest values observed in the remanent magnetization for all phases below T_N should correspond to the temperature at which the difference in magnetization of the two sublattices is higher. The saturation of the magnetic moments of both ferromagnetic sublattices to the total moment of the Fe(III) ions would lead to the disappearance of the remanent magnetic moment at lower temperatures. However, in the title compounds the remanent magnetization does not tend towards zero at 0 K, as could be expected if only ferrimagnetic behavior was present. Consequently, an additional factor, such as a slight canting of the magnetic moments of the Fe(1) and Fe(2) sublattices in the ordered state should be considered. This fact gives rise to the presence of a weak ferromagnetic moment in the compounds. Considering the observed values for the remanent magnetization, the magnitude of the slight misalignment should be of a few tenths of a degree, in every case. Likewise, the canting angle should decrease with increasing x in the $Li_3Fe_2(AsO_4)_{3-x}(PO_4)_x$ solid solution becoming practically negligible for the $Li_3Fe_2(PO_4)_3$ phase (see ref. 21). Finally, it can be concluded that the increase of the tilt angle between the $Fe(1)O_6$ and $Fe(2)O_6$ octahedra with increasing arsenate content in $Li_3Fe_2(AsO_4)_{3-x}(PO_4)_x$ leads to a phenomenon of canting, that is hampered in the case of $Li_3Fe_2(PO_4)_3$, probably due to the existence of pseudosymmetry between the $Fe(1)O_6$ and $Fe(2)O_6$ octahedra.

Acknowledgements

This work has been carried out with the financial support of the Ministerio de Educación y Ciencia (PB97-0640) and the UPV/EHU (UPV 169.310-EB149/98) which we gratefully acknowledge. One of us (G.E.B.) works within the ICTP (Trieste) Associate Scheme. This work was also partially supported by the Gobierno Vasco, and CAPES and CNPq (Brazil).

References

1 S. E. Sigaryov and V. G. Terziev, *Phys. Rev. B*, 1993, **48**, 16252.
2 V. V. Kravchenko and S. E. Sigaryov, *Solid State Commun.*, 1992, **83**, 149.
3 A. B. Byov, A. P. Chirkin, L. N. Demyanets, S. N. Doronin, E. A. Genika, A. K. Ivanov-Shits, I. P. Kondratyuk, B. A. Maksimov, O. K. Mel'nikov, L. N. Mudaryan, V. I. Simonov and V. A. Timofeeva, *Solid State Ionics*, 1990, **38**, 31.
4 I. A. Verin, E. A. Genkina, B. A. Maksimov, L. A. Muradyan and M. I. Sirota, *Sov. Phys. Crystallogr.*, 1985, **30**, 394.
5 M. Pintard-Scrépel, F. d'Yvoire and E. Bretey, *Solid State Chem. Proc. Eur. Conf. 2nd 1982*, 1982, 215.
6 H. Y.-P. Hong, *Mater. Res. Bull.*, 1976, **11**, 173.
7 M. d'Yvoire, M. Pintard-Scrépel, E. Bretey and M. de la Rochère, *Solid State Ionics*, 1983, **9–10**, 851.
8 M. Pintad-Scrépel, F. d'Yvoire and F. Remy, *C. R. Acad. Sci.*, 1978, **C286**, 381.
9 M. H. Rapposch, J. B. Anderson and E. Kostiner, *Inorg. Chem.*, 1980, **19**, 3531.
10 D. Beltran-Porter, R. Olazcuaga, C. Delmas, F. Cherkaoui, R. Brochu and G. Le Flem, *Rev. Chim. Mineral.*, 1980, **17**, 458.
11 C. Greaves, P. R. Slater, M. Slaska and C. M. Muirhead, *Physica B*, 1994, **194–196**, 199.
12 N. Fanjat and J. L. Soubeyroux, *J. Magn. Magn. Mater.*, 1992, **104–107**, 933.
13 G. J. Long, G. Longworth, P. Battle, A. K. Cheetham, R. V. Thundathil and D. Beveridge, *Inorg. Chem.*, 1979, **18**, 624.
14 H. Y. Chen, *Mater. Res. Bull.*, 1979, **14**, 1583.
15 Z. Jirak, R. Salmon, L. Fournes, F. Menil and P. Hagenmuller, *Inorg. Chem.*, 1982, **21**, 4218.
16 P. D. Battle, A. K. Cheetham, G. J. Long and G. Longworth, *Inorg. Chem.*, 1982, **21**, 4223.
17 R. Salmon, R. Olazcuaga, Z. Jirak, D. Beltran-Porter, L. Fournes, F. Menil and G. Le Flem, *Solid State Chem. Proc. Eur. Conf. 2nd 1982*, 1982, 567.
18 C. C. Torardi and E. Prince, *Mater. Res. Bull.*, 1986, **21**, 719.
19 W. M. Reiff, J. H. Zhang and C. C. Torardi, *Solid State Chem.*, 1986, **62**, 231.
20 W. M. Reiff, J. H. Zhang, H. Tam, J. P. Attfield and C. C. Torardi, *J. Solid State Chem.*, 1997, **130**, 147.
21 A. Goñi, L. Lezama, N. O. Moreno, L. Fournes, R. Olazcuaga, G. E. Barberis and T. Rojo, *Chem. Mater.*, 2000, **12**, 62.
22 J. Rodriguez Carvajal, FULLPROF program, Rietveld pattern matching analysis of powder patterns, 1994.
23 K. Nakamoto, *Infrared and Raman Spectra of Inorganic and Coordination Compounds*, 5th Edition, John Wiley and Sons, New York, 1997.
24 A. Bencini and D. Gatteschi, *EPR of exchange coupled systems*, Springer-Verlag, Berlin, 1990.